Polymer Testing 89 (2020) 106710

Contents lists available at ScienceDirect

Polymer Testing

journal homepage: http://www.elsevier.com/locate/polytest

Mechanical properties and electrical surface charges of microfibrillated cellulose/imidazole-modified polyketone composite membranes

Pablo Gonzalez Cortes [a], Rodrigo Araya-Hermosilla [b,**], Esteban Araya-Hermosilla [c], Daniela Acuña [a], Andreas Mautner [d], Leonardo Caballero [e], Francisco Melo [e], Ignacio Moreno-Villoslada [f], Francesco Picchioni [g], Aldo Rolleri [h], Franck Quero [a,i,*]

[a] Laboratorio de Nanocelulosa y Biomateriales, Departamento de Ingeniería Química, Biotecnología y Materiales, Facultad de Ciencias Físicas y Matemáticas, Universidad de Chile, Avenida Beauchef 851, Santiago, Chile
[b] Programa Institucional de Fomento a la Investigación, Desarrollo e Innovación, Universidad Tecnológica Metropolitana, Ignacio Valdivieso 2409, P.O. BOX 8940577, San Joaquín, Santiago, 8940000, Chile
[c] Center for Micro-BioRobotics, Istituto Italiano di Tecnologia Viale Rinaldo Piaggio 34, Pontedera, PI, 56025, Italy
[d] Polymer and Composite Engineering (PaCE) Group, Institute of Materials Chemistry and Research, Faculty of Chemistry, University of Vienna, Währinger Straße 42, A-1090, Vienna, Austria
[e] Departamento de Física, Universidad de Santiago de Chile, Avenida Ecuador, 3493, Santiago, Chile
[f] Laboratorio de Polímeros, Instituto de Ciencias Químicas, Facultad de Ciencias, Isla Teja, Universidad Austral de Chile, Valdivia, Chile
[g] Department of Chemical Engineering, ENTEG, University of Groningen, Nijenborgh 4, 9747AG, Groningen, the Netherlands
[h] Laboratorio de Productos Forestales, Instituto de Bosques y Sociedad, Facultad de Ciencias Forestales y Recursos Naturales, Universidad Austral de Chile, Valdivia, Chile
[i] Millennium Nucleus on Smart Soft Mechanical Metamaterials, Avenida Beauchef 851, Santiago, 8370456, Chile

ARTICLE INFO

Keywords:
Microfibrillated cellulose
Polyketone
Paal-knorr reaction
Composite membrane
Mechanical properties
Electrical surface charges

ABSTRACT

In the present work, microfibrillated cellulose (MFC) suspensions were produced by high-pressure homogenization and subsequently used to fabricate MFC membranes (C-1) by vacuum filtration followed by hot-pressing. A polyketone (PK50) was chemically modified by Paal-Knorr reaction to graft imidazole (IM) functional groups along its backbone structure. The resulting polymer is referred to as PK50IM80. By solution impregnation, C-1 was immersed in an aqueous solution of PK50IM80 and subsequently hot pressed, resulting in the fabrication of MFC/PK50IM80 composite membranes (C-IMP). Another method, referred to as solution mixing, consisted in adding MFC into an aqueous solution of PK50IM80 followed by vacuum filtration and hot-pressing to obtain MFC/PK50IM80 composite membranes (C-MEZC). C-IMP and C-MEZC were characterized by a wide range of analytical techniques including, X-ray photoelectron spectroscopy, Fourier-transform infrared chemical imaging, scanning electron microscopy, atomic force microscopy, dynamical mechanical analysis, tensile testing as well as streaming zeta potential, and compared to C-1 (reference material). The results suggested that C-IMP possess a more homogeneous distribution of PK50IM80 at their surface compared to C-MEZC. C-IMP was found to possess significantly enhanced Young's modulus compared to C-1 and C-MEZC. The tensile strength of C-IMP was found to improve significantly compared to C-1, whereas C-1 possessed significantly higher tensile index than C-IMP and C-MEZC. Furthermore, the presence of PK50IM80 at the surface of MFC was found to significantly shift the isoelectric point (IEP) of the membranes from pH 2.3 to a maximum value of 4.5 for C-IMP. Above the IEP, C-IMP and C-MEZC were found to possess significantly less negative electrical surface charges (plateau value of −25 mV at pH 10) when compared to C-1 (plateau value of −42 mV at pH 10). Our approach may have implication to broaden the range of filtration applications of MFC-based membranes.

* Corresponding author. Laboratorio de Nanocelulosa y Biomateriales, Departamento de Ingeniería Química, Biotecnología y Materiales, Facultad de Ciencias Físicas y Matemáticas, Universidad de Chile, Avenida Beauchef 851, Santiago, Chile.
** Corresponding author.
E-mail addresses: rodrigo.araya@utem.cl (R. Araya-Hermosilla), fquero@ing.uchile.cl (F. Quero).

https://doi.org/10.1016/j.polymertesting.2020.106710
Received 6 April 2020; Received in revised form 1 June 2020; Accepted 20 June 2020
Available online 4 July 2020

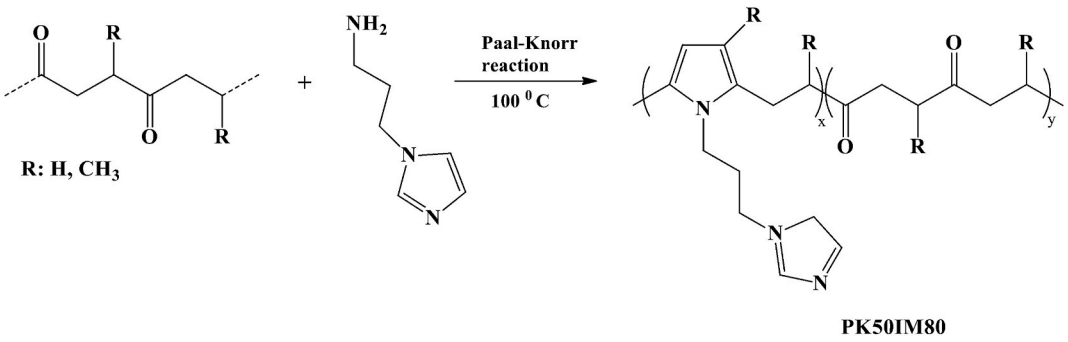

Fig. 1. Schematic representation of the chemical modification of PK50 with imidazole by Paal-Knorr reaction.

1. Introduction

Materials derived from natural resources, including cellulose, are particularly relevant to design greener products, e.g. composite materials [1,2]. Cellulose is one of the most abundant, renewable and biodegradable polymers available on earth [3]. From this raw material, microfibrillated cellulose (MFC) can be obtained [4]. MFC is commonly produced by high-pressure mechanical processes including high-pressure homogenization and microfluidization [5]. MFC is constituted of a mixture of several grades of cellulose nanofibers (CNFs), each of them having different size distribution dimensions including height, width and length. It usually comes in the form of an aqueous gel-like substance, whose viscosity can be controlled by adjusting its solid content [6]. The width distribution of finer fractions of MFC fibres is relatively wide with lower values close to 20 nm and higher values that can go up to 300 nm [7]. Their length is typically of several microns [5,8]. CNFs have been used as building blocks to fabricate a range of cellulose-based materials including aerogels [9,10], hydrogels [10], macrofibres [11], nanocomposites [12] and membranes [13], to name a few. Membranes made of CNFs are also referred to as nanopapers in the literature [13]. These membranes possess high tensile mechanical properties [14], low thermal expansion coefficient [15], high oxygen barrier performance [16,17] as well as adequate permeability [18,19]. This equips fibrillated cellulose membranes with relevant features for their applications in separation processes including water treatment [13,20]. For the removal of chemical species including cations Ca^{2+} and Mg^{2+}, cellulose membranes do not possess adequate pore size (typically from 40 to 300 nm), which is too large for the efficient removal of these chemical species from water by size exclusion [21]. Moreover, their adsorption capacity has been reported to be low since the hydroxyl groups available at the surface of MFC exhibit limited electrostatic interactions with cations [20].

A strategy that has been proposed to overcome this issue is to chemically modify the surface of cellulose fibres by introducing functional groups [13,20]. These chemical groups can tune the magnitude of the negatively charged surfaces over a wide range of pH to better match the magnitude of the positive charges of targeted cations and improve selective adsorption efficiency [22]. This strategy was found to improve significantly the removal efficiency of cellulose membranes [20]. Fine control over the magnitude of the electrical surfaces of polymeric membranes has been reported to be crucial for efficient separation, especially when the solute size is much smaller than pore size [23]. Direct chemical modification of cellulose fibres exhibits, however, several drawbacks since these chemical modifications commonly require the use of expensive solvents and chemicals as well as additional steps. Another drawback is that typically only the hydroxyl group positioned at C6 in the molecular structure of cellulose is available for chemical modification owing to its higher reactivity [24]. As a result, higher degrees of substitution than 1 cannot be facilitated, which in turn limits the removal efficiency.

A potential approach to overcome this is the combination of CNFs with amorphous polymers bearing numerous functional chemical groups able to interact with positively charged chemical species, without sacrificing the specific surface area and mechanical properties of the resulting membrane. The latter is particularly challenging since the intercalation of polymer in between MFC fibres might disrupt the effective mechanical performance of the cellulose membranes as it has been suggested before for bacterial cellulose (BC)/polyvinyl alcohol (PVA) nanocomposites [25]. In addition to increasing the number of interactions with cationic species, the polymer could potentially help controlling membrane pore size, depending on the composite membrane fabrication method used, to make them more suitable for separating cationic chemical species from water by size exclusion. This could result in the formation of composite membranes that would treat water by three mechanisms: (i) electrostatic and (ii) chelating interactions as well as (iii) size exclusion.

Various composite manufacturing methods have been reported to combine cellulose fibres with polymers. These include melt extrusion [26], vacuum impregnation [27], compression moulding [28], solvent casting [26], in-situ biosynthesis [25], solution impregnation [25] and solution mixing [29,30], to cite only a few. Each method possesses its advantages and drawbacks, which need to be taken into account depending on various parameters including the polymer to be used and its targeted application. One of the advantages of solution impregnation and solution mixing methods is that they are both compatible with papermaking production methods. Up to date, various polymers have been combined with MFC fibres with the aim of improving mechanical properties as well as providing new properties or functionalities [31]. These include, among others, polyvinyl alcohol [25], polylactide [28,32,33], cellulose acetate butyrate [34], polymethylmethacrylate [35] or acrylic resins [27].

Polyketones (PKs) are a family of polymers that so far have not been evaluated regarding the generation of cellulose fibre-containing composites. PKs are produced by copolymerization of carbon monoxide (CO), a toxic product of combustion reactions, in controlled stoichiometric proportions with unsaturated hydrocarbons monomers (propylene and ethylene) [36]. These thermoplastic polymers offer several advantages over others. PKs can be chemically modified by Paal-Knorr reaction under mild experimental conditions, where high-conversion degree (up to 80%) of 1,4 dicarbonyl groups can be obtained [37]. This results in the introduction of numerous functional groups including amine and imidazole moieties along the backbone structure of PKs [37]. The Paal-Knorr reaction is a simple and inexpensive route that introduces pyrrole rings along with other functional or multi-functional groups into the macromolecular structure of PKs [37–40]. This has been reported to allow for obtaining chemically modified PKs with imidazole pendant groups that possess excellent ability to remove cationic chemical species from water [41].

The present study focuses on introducing, for the first time, imidazole moieties onto the surface of cellulose nanofibers by combining MFC with imidazole-chemically-modified-PK (PK50IM80). This was performed by two methods: solution impregnation and solution mixing,

resulting in the fabrication of novel composite membranes. We propose that the mechanical properties and the magnitude of the electrical surface charges of MFC/PK50IM80 membranes can be modified by combining MFC fibres with PK50IM80 that possesses controlled amounts of amine and imidazole moieties along its polymer backbone. This approach will potentially help obtaining MFC-based membranes with various electrical surface charge features to allow widening their range of filtration applications.

2. Materials and method

2.1. Materials

Commercial bleached eucalyptus cellulose pulp (solid content = 13.5%) having an α-cellulose content of 90.2% was kindly supplied by CMPC (Nacimiento, Chile) and used as received to produce MFC. The sugar composition of the pulp was quantified by high performance liquid chromatography and found to be 74.2% glucans, 14.8% xylans and 0.8% arabinans among other constituents. Polyketone (PK50) with a total olefin ratio of 50% ethylene and 50% propylene (PK50, Mw 3636 Da), was chemically modified with 1-(3-aminopropyl)-imidazole (IM) (Mw 125.17 Da) (Sigma-Aldrich, The Netherlands) via Paal-Knorr reaction (Fig. 1). This modified PK50 polymer is referred to as PK50IM80. IM80 indicates that PK50 has been modified with IM with a 1,4 dicarbonyl conversion aiming at 80% [37] (see Supplementary Data for more details). Distilled water was used in all experiments unless specified otherwise.

2.2. Production of never-dried microfibrillated cellulose

Never-dried MFC was obtained by high-pressure homogenization of bleached eucalyptus cellulose pulp. Initially, a volume of 13.6 mL of eucalyptus pulp (solid content 13.5%) was added to 486 mL of milliQ water. The mixture was then subjected to two successive homogenization passes using a kitchen blender (TH-850 D, Thomas, Germany) to disperse the pulp into water (5 min at 31 000 rpm each). The aqueous suspension of cellulose was subsequently homogenized using a high-shear homogenizer (T-25 Digital Ultraturrax, IKA, USA) for 10 min at 13 000 rpm. Finally, the suspension, having a solid content of 0.5%, was homogenized by 6 successive passes through a double chamber high-pressure homogenizer (SPX, APV-2000, Denmark) at a pressure of ~1000 bars. The final aqueous suspension with a solid content of 0.48 wt% was stored in a refrigerator (~4 °C) until further use.

2.3. Fabrication of microfibrillated cellulose membranes

30 mL of MFC suspension (solid content of 0.48 wt%) was vacuum filtered for ~30 min using polyvinylidene fluoride filters (45 mm diameter, 0.22 μm pore size, Durapore, Ireland) and a vacuum pump (Rocker 400, Taiwan). At the end of the filtration process, a wet filter cake was obtained that was subsequently sandwiched between two fine metallic meshes and pressed at a pressure of 6 MPa for 10 min to remove the excess of water. The resulting membrane was subsequently dried for 30 min at 100 °C using a heat-press (Rheinstern, Germany). The obtained MFC membrane is referred to as C-1 and corresponds to our reference material throughout the entire study. The grammage of the membranes (~40 mm in diameter) was determined by calculating the ratio between their weight (g) and surface area (m^2). The thickness of the membranes was measured using a digital micrometer gauge (Accud, 0–25 mm, resolution 0.001 mm, Japan).

2.4. Preparation of microfibrillated cellulose/polyketone composite membranes

An aqueous solution of 10 mg/mL PK50IM80 was prepared by adding 500 mg of PK50IM80 into 50 mL of distilled water in a glass beaker. A few drops (0.03 mL each) of acetic acid were added to adjust the pH of the polymer solution to 5 to facilitate the dissolution of PK50IM80.

The first method for the preparation of each composite membrane was immersion of an MFC membrane in 10 mL of the previously prepared PK50IM80 solution for 20 min. Each impregnated membrane was squeezed for 10 min between filter paper and metal plates under a weight of 10 kg to gently remove the excess of water and pressed at 6 MPa for 10 min and finally dried for 30 min at 100 °C using a heat-press (Rheinstern, Germany). This fabrication method is referred to as "solution impregnation" and the resulting composite membranes are referred to as C-IMP. The PK50IM80 content present in C-IMP was calculated from the weight difference between oven-dried MFC membranes before and after impregnation. An average weight content value of 3.8 ± 0.01% was obtained.

A second method was used to prepare composite membranes. For this, 30 mL of MFC suspension (solid content of 0.48 wt%) was mixed with 10 mL of the PK50IM80 solution (~10 mg/L). The mixture was magnetically stirred for 10 min and vacuum filtered (Rocker 400, Taiwan) using polyvinylidene fluoride filter discs (45 mm diameter, 0.22 μm pore size, Durapore, Ireland). The wet filter cake was first squeezed for 10 min between filter papers and metal plates under a weight of 10 kg and kept under a pressure of 6 MPa for 10 min to further remove most of the excess of water. Finally, each membrane was dried for 30 min at 100 °C using a heat-press (Rheinstern, Germany). The composite membranes obtained using this method are referred to as C-MEZC. The PK50IM80 content present in C-MEZC was estimated from the difference between the solid weight content present in the 30 mL of MFC suspension and the weight of oven-dried C-MEZC. An average weight content value of 1.7 ± 0.01% was obtained. The porosities (P) of C-1, C-IMP and C-MEZC membranes were determined using equation [42]:

$$P = \left(1 - \frac{\rho_{membrane}}{\rho_{cellulose}}\right) \times 100 \quad (1)$$

where $\rho_{membrane}$ corresponds to the bulk density of the membrane and $\rho_{cellulose}$ corresponds to the density of cellulose with a value of 1.46 g cm^{-3} [43]. The porosity values obtained may overestimate the porosity of the membranes since the real density cellulose can be lower than 1.46 g cm^{-3}.

2.5. Characterization of MFC and the composite membranes

2.5.1. Morphology of microfibrillated cellulose by atomic force microscopy

The morphology and size distribution dimensions including height, width and length of the MFC fibres contained in MFC suspensions was assessed by atomic force microscopy (AFM). An aqueous suspension of MFC (0.48 wt%) was diluted to 10 mL to reach a final concentration of ~0.01 wt% by adding Milli-Q water. The suspension was subsequently sonicated using an ultrasonic probe (Misonix XL 2020, USA) for 2 min at 25 W. Then a few μL drops of the sonicated MFC suspensions were deposited onto a mica substrate and air-dried under ambient conditions prior to imaging. The height, width and length size distributions were estimated by performing 100 individual measurements.

2.5.2. Surface chemical analysis by FTIR microscopy

The molecular structure and 2D chemical images of the surface of MFC and composite membranes were assessed using FTIR spectroscopy and microscopy, respectively. The system consisted of a spectrometer (Frontier, PerkinElmer, USA) with two DTGS NIR and MIR detectors, both covering a range between 14700 and 350 cm^{-1} with a spectral resolution of 4 cm^{-1}. The imager (Spotlight 400, PerkinElmer, USA) was equipped with a detector type MCT MIR (7800-720 cm^{-1}) with a resolution greater than 2 cm^{-1}. ATR-FTIR imaging mode with a pixel resolution of 1.56 μm, resolution of 16 cm^{-1}, 16 scans and diffuse reflectance

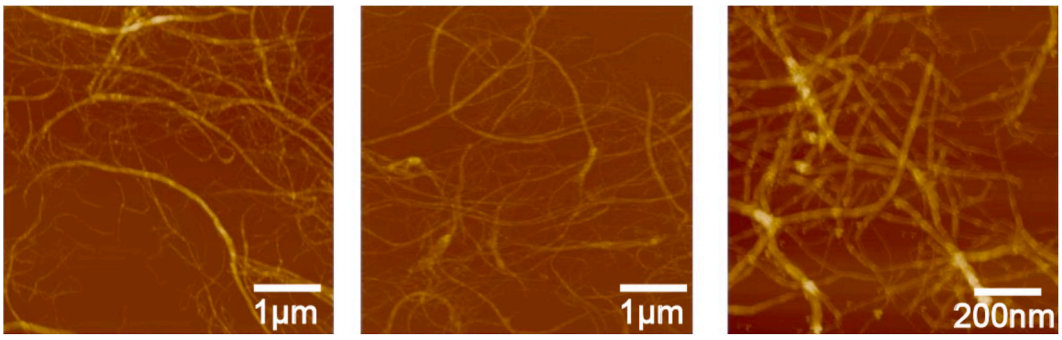

Fig. 2. Atomic force microscopy (AFM) images of microfibrillated cellulose fibres obtained by high-pressure homogenization.

mode with a pixel resolution of 6 μm resolution of 16 cm^{-1} and 16 scans were used to generate the spectra, as well as surface chemical images. The chemical images were corrected from atmospheric contributions. To assure repeatability, the sample mounted onto the platform was first scanned in visible mode to select the position to be subsequently assessed by FTIR microscopy. The coordinates of the selected position allowed to return to the exact same study area.

2.5.3. Surface elemental composition by X-ray photoelectron spectroscopy

The elemental surface composition of MFC (C-1) and composite membranes (C-IMP and C-MEZ) was quantified by X-ray photoelectron spectroscopy (XPS) using Al Kα X-rays as source, a spot size of 400 μm and an energy step size of 1 eV for the survey and 0.1 eV for detailed analysis, respectively, on a Thermo Scientific Nexsa Photoelectron Spectrometer. Samples were etched for 60 s using a low-energy Ar cluster (6000 eV, 1000 atom clusters) prior to analysis to clean the surface of the sample.

2.5.4. Surface morphology by field emission scanning electron microscopy

The surface morphology of MFC and composite membranes was observed by field emission scanning electron microscopy (FESEM, Inspect F50, FEI, USA) and atomic force microscopy (AFM). SEM images were acquired using an acceleration voltage of 5–10 kV according to image acquisition. The samples were gold coated under vacuum for 10 min resulting in the deposition of a 5 nm gold layer at their surface. The surface atomic composition of the samples was identified by energy dispersive X-ray spectroscopy. AFM height and maximum force images were acquired by fast force mapping mode using a Jupiter XR system (Asylum Research – an Oxford Instruments Company, Santa Barbara, CA). Asylum Research cantilevers were used with a nominal force constant of 6 Nm^{-1} and a resonance frequency of 1500 kHz. All cantilevers had a reflective coating on their back side.

2.5.5. Crystalline structure by powder X-ray diffraction

The crystalline structure of the MFC and composite membranes was investigated by powder X-ray diffraction. Each diffractogram was generated using a diffractometer (Bruker D8 Advance, United Kingdom) equipped with a monochromatic radiation source of Cu Kα radiation (λ = 1.54 Å) at 40 kV and 30 mA and a step time of 0.02° each 0.1 s in the diffraction angle 2θ range of 5–80°. The diffraction patterns of the samples were processed using Origin Pro Software.

2.5.6. Thermal stability by thermogravimetric analysis

Thermogravimetric analysis (TGA) was conducted using a thermal analyser (TA instruments model Q50, USA). Each sample having an initial mass of ~10 mg was subjected to a temperature range of 20–800 °C at a heating rate of 10 °C min^{-1} under nitrogen atmosphere with a flow rate of 40 mL min^{-1}.

2.5.7. Thermomechanical properties by dynamic mechanical analysis

The thermomechanical performance of MFC and composite membranes was determined by dynamic mechanical analysis (DMA, PerkinElmer DMA 8000, country) with a heating rate of 3 °C min^{-1} at a constant frequency of 1 Hz. The samples (thin strips having dimensions of 5 × 20 × 0.07 mm) were analysed in the temperature range of 0–200 °C.

2.5.8. Tensile mechanical properties

Tensile mechanical properties of the MFC and composite membranes were determined using a universal tensile testing machine (Zwick/Roell Z005, Germany). Tests were performed on strips (~20 mm × 1 mm × 0.06 ± 0.01 mm) cut from the fabricated membranes using razor blades. Prior to analysis, the strips were mounted onto cardboard testing cards and glued using two-part epoxy glue. The temperature and the relative humidity were of 25 °C and 48%, respectively. The thickness of each specimen was measured at three different locations along the length of the sample using a digital micrometer gauge (Accud, 0–25 mm, resolution 0.001 mm). The crosshead displacement speed of the tensile tester was set to 1 mm min^{-1} and the gauge length was of 20 mm. At least 5 samples were tested for each material. Average values are reported along with their associated standard deviations used as error values.

2.5.9. Specific surface area by inverse gas chromatography

The specific surface area of MFC membranes (C-1) and composite membranes (C-IMP and C-MEZ) was assessed by inverse gas chromatography (iGC) at 30 °C and 0% RH using a surface energy analyser (Surface Measurement Systems, London, UK). ~200 mg of membrane strips (3 mm wide) were cut and inserted into a measurement column (inner diameter 4 mm, outer diameter 6 mm). The specific surface area of the samples was then determined by octane retention at various coverages resulting in $p/p0p_0$ of 0.05–0.35, with the specific surface area being computed using the Brunauer-Emmett-Teller (BET) model from the centre of mass of the peaks.

2.5.10. Magnitude of electrical surface charges by streaming zeta-potential

The magnitude of electrical surface charges of MFC (C-1) and composite membranes (C-IMP and C-MEZ) was quantified by measuring ζ-potential as function of pH using an electrokinetic analyser (Anton Paar SurPASS, Graz, Austria) in an adjustable gap cell (~150 μm). The electrolyte solution (1 mM KCl) was pumped through the cell at pressures steadily increasing up to 300 mbar and the ζ-potential determined from the streaming current. The pH was controlled by titrating 0.05 mol L^{-1} KOH and HCl, respectively, into the electrolyte solution. Four measurement points were obtained for each sample and average values are reported along with their associated standard deviations used as error values.

3. Results and discussion

The morphology of the MFC fibres prepared by high-pressure homogenization was assessed by atomic force microscopy (AFM). AFM images are displayed in Fig. 2. The dimensions of MFC fibres are

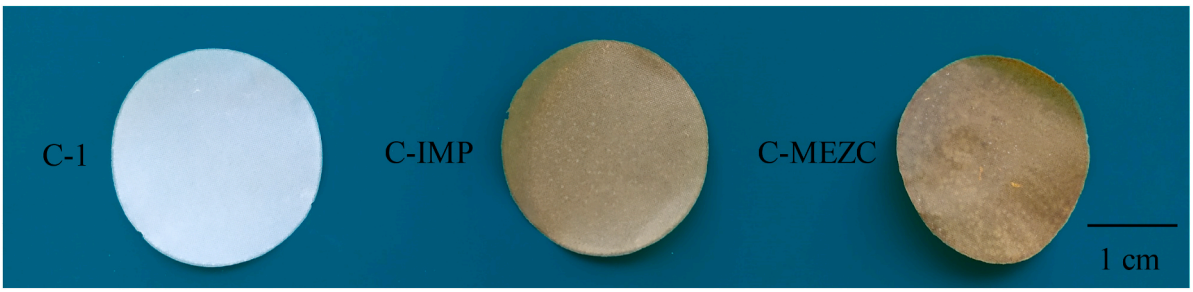

Fig. 3. Photograph of MFC membrane (C-1) and composite membranes prepared by solution impregnation (C-IMP) and solution mixing (C-MEZC).

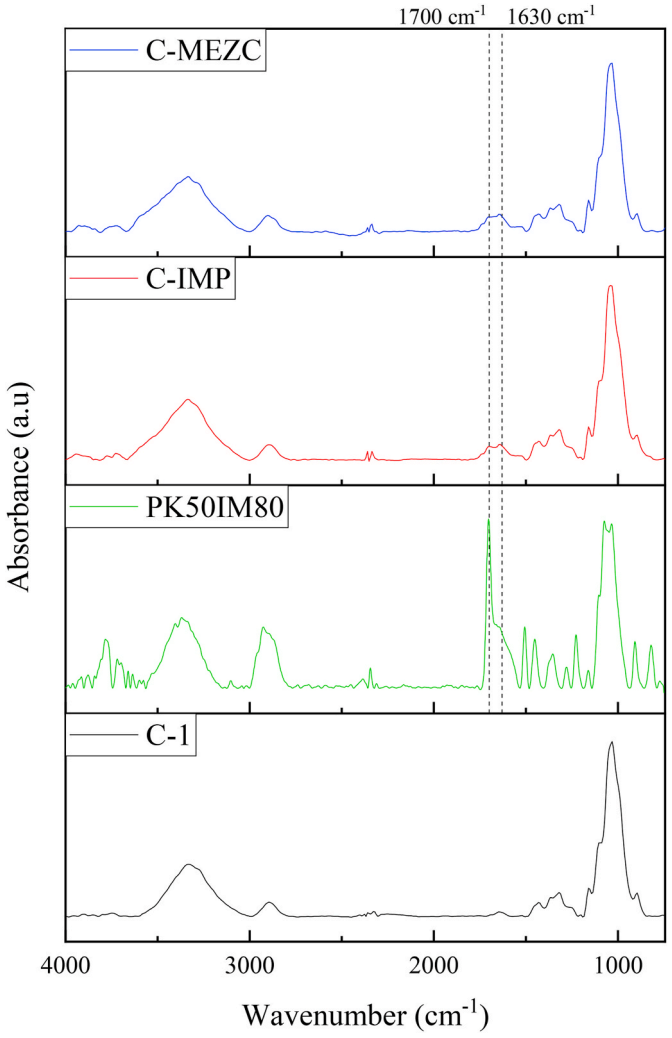

Fig. 4. FTIR spectra of MFC membrane (C-1), polyketone chemically modified (P50IM80) and composite membranes (C-IMP and C-MEZC) using attenuated total reflectance (ATR). The black pointed line indicates the presence of the carbonyl absorption band in PK50IM80, C-IMP and C-MEZC.

influenced by many factors including raw material, chemical and enzymatic treatments [44]. The images show the typical MFC fibre bundle morphology as reported before in the literature for MFC fibres derived from eucalyptus pulp [45]. From these images the height, width and length size distributions of the fibres were determined. These are reported in Fig. S1. Their height and width varied from 5 to 40 nm and 30–280 nm, respectively, whereas their length varied from ~500 nm to 6 μm.

Table 1
Binding energy (BE) and elemental atomic concentration obtained from high resolution X-ray photoelectron for microfibrillated cellulose membrane (C-1) and composite membranes prepared by solution impregnation (C-IMP) and solution mixing (C- MEZC).

Material	Binding energy (eV)			Elemental atomic composition (%)		
	C 1s	N 1s	O 1s	C 1s	N 1s	O 1s
C-1	284.8	399.5	532.3	67.1	0.4	32.5
C-IMP	284.9	399.7	532.3	65.9	2.2	32.0
C-MEZC	285.7	399.8	532.4	65.7	2.0	32.3

A photograph of MFC and composite membranes is shown in Fig. 3. MFC membranes were white as typical for bleached eucalyptus pulp. For both C-IMP and C-MEZC composite membranes a brownish color was observed, which was related to the incorporation of PK50IM80 within the MFC fibre network. Table S1 reports thickness, bulk density, grammage and density values obtained for C-1, C-IMP and C-MEZC membranes.

Figs. S2a and S2b show FTIR spectra of PK50IM80 and MFC (C-1), respectively, with bands being summarized in Table S3. For PK50IM80 an absorbance band located at a wavenumber position of ~3100 cm^{-1} was associated to the stretching of the protons in the pyrrole ring C=C-H [46]. In the wavenumber range of 2900-2850 cm^{-1}, absorption peaks associated with the stretching mode of the CH (alkyl) groups of the PK backbone were noted [47]. At a wavenumber position of ~1700 cm^{-1}, an absorption band related to the vibrational motions of carbonyl groups present in the polyketone backbone structure was also observed [40]. At a wavenumber position of ~1650 cm^{-1} an absorption peak associated with the vibrational motions of C=C that belong to pyrrol ring structures of PK50IM80 appeared [40]. The full spectroscopical description of PK50IM80 can be found in Supplementary Data (Figs. S3 and S4).

For MFC (C-1), an absorption band located at a wavenumber position of ~3330 cm^{-1} was associated to the stretching vibrations of OH groups in the cellulose [46], whereas the bands located between 2900 and 2800 cm^{-1} and ~1638, 1427, 1157, 1020 and 893 cm^{-1} were related to vibrational motions of moieties that belong to the molecular structure of cellulose [46].

FTIR-ATR spectra of MFC (C-1) and composite membranes (C-IMP and C-MEZC) are shown in Fig. 4 and the full assignment information is reported in Table S2. For C-IMP and C-MEZC membranes, it was possible to observe an absorption band located at a wavenumber position of ~1700 cm^{-1} as indicated by the black arrows. This band relates to the vibrational motion of carbonyl moieties [40]. This confirmed that PK50IM80 was adsorbed at the surface of MFC fibres during the preparation of the composite membranes. The relative intensity of the carbonyl absorption band obtained from the composite membranes was, however, lower than for PK50IM80 due to the dilution effect, as expected (3.8 and 1.7% of PK50IM80 for C-IMP and C-MEZC, respectively).

The elemental composition at the surface of MFC and composite

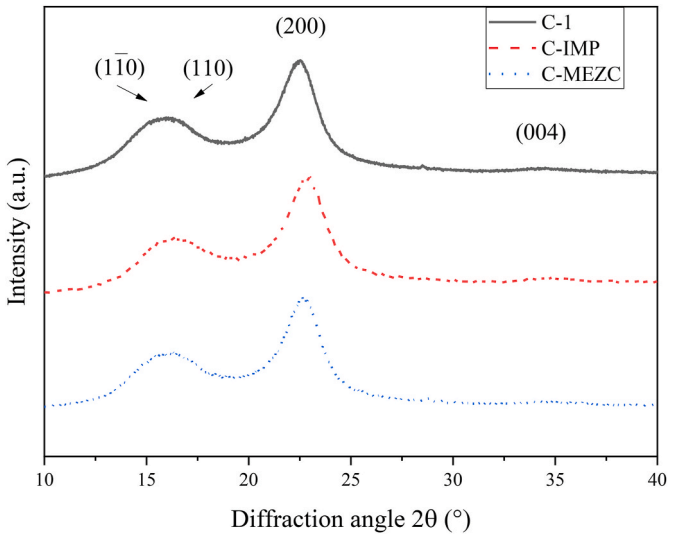

Fig. 5. Powder X-ray diffraction patterns of microfibrillated cellulose membrane (C-1, black full line) and composite membranes prepared by solution impregnation (C-IMP, red dashed line) and solution mixing (C- MEZC, blue dotted line).

membranes was quantified by X-ray photoelectron spectroscopy (XPS). The corresponding data are reported in Table 1. In Fig. S5 XPS low-resolution survey spectra for C-1, C-IMP and C-MEZC are shown. The spectrum of C-1 displays the signal of C 1s, N 1s and O 1s, while C-IMP and C-MEZC exhibited similar signals but with a more intense signal peak for N 1s, indicating the presence of PK50IM80. In Fig. S6a, the high-resolution C 1s spectrum for the C-1 in the binding energy range of 280–298 eV is shown. Two peaks, located at ~284.5 and 286.0 eV, attributed to C-C and C-O moieties, respectively, were found. For the spectra of C-IMP and C-MEZC (Figs. S6b and S6c) the peak located, respectively, at ~284.9 and 285.7 eV correspond to the binding energy of C 1s in C-C bonds was more intense when compared to C-1. This was explained by the presence of PK50IM80 located at the surface of C-IMP and C-MEZC composite membranes that exhibited a higher carbon content than cellulose, due to a high amount of C-C bonds along the backbone structure of PK50IM80 (compare Fig. 1). Table 1 reports the binding energy (BE) and atomic composition (%) obtained for C-1, C-IMP and C-MEZC. The fractions of nitrogen were 0.4, 2.2 and 2.0%, respectively. This increase in nitrogen content measured at the surface of C-IMP and C-MEZC was associated to the presence of PK50IM80, which was similar albeit slightly higher for C-IMP compared to C-MEZC. This confirms the similar PK50IM80 wt contents present in both C-IMP and C-MEZC composite membranes.

Powder X-ray diffraction patterns obtained for C-1, C-IMP and C-MEZC membranes are shown in Fig. 5. The diffraction peaks located at diffraction angle positions of 2θ = ~15, ~16, ~23 and ~35° corresponded to the diffraction planes (110), (110), (200) and (004), respectively [48]. This indicated that the polymorph of the cellulose source corresponded mainly to the cellulose Iβ crystalline form as it is usually the case for plant cellulose [48]. Moreover, the diffraction patterns demonstrated that the composite fabrication methods did not affect the crystalline structure of MFC fibres. It is important to preserve as much as possible thermal and mechanical properties of MFC fibres that both rely on crystallinity in order to realize appropriate thermal and mechanical properties in the composite materials, too. No additional

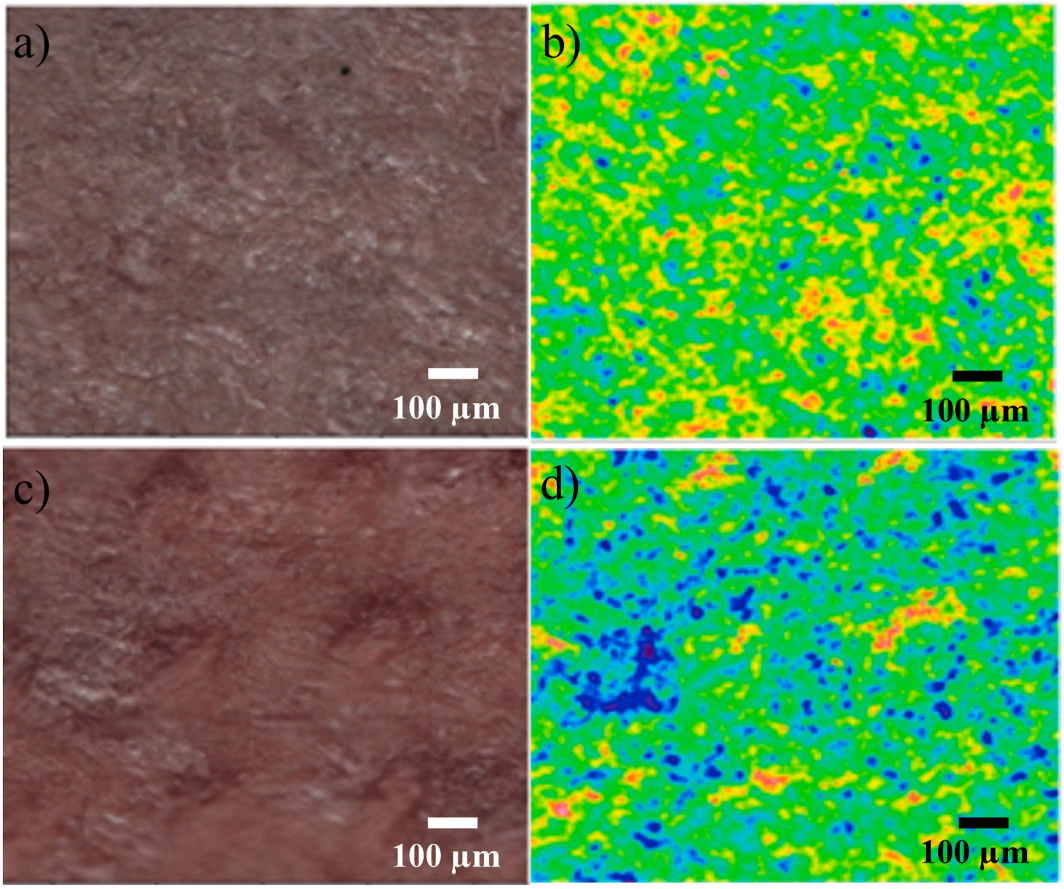

Fig. 6. Optical and FTIR chemical images of composite membranes prepared by solution impregnation C-IMP (a,b) and solution mixing C-MEZC (c,d) showing the distribution of PK50IM80 at their surface. The concentration of PK50IM80 increases in the color order: blue < green < yellow < red.

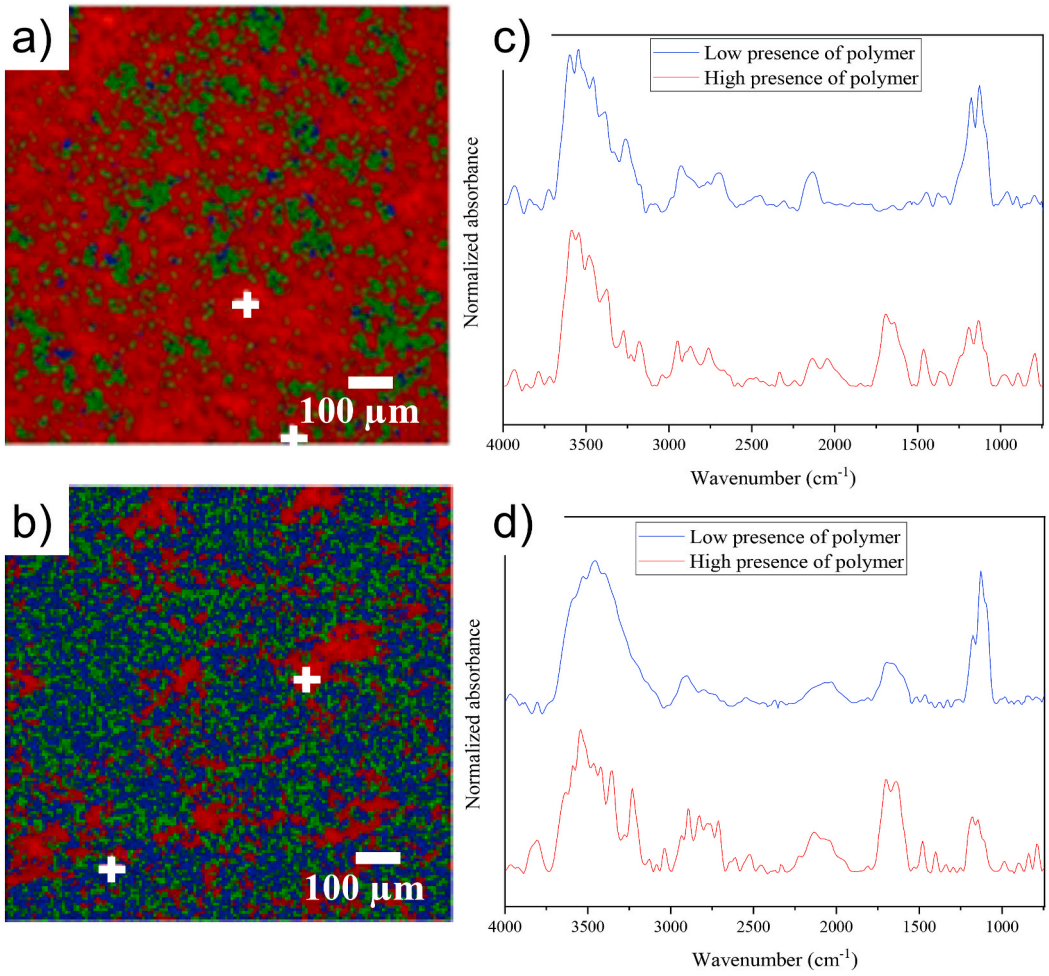

Fig. 7. Principal component analysis (PCA) images of the spatial distribution of PK50IM80 at the surface of a) impregnated (C-IMP) and b) mixed (C-MEZC) composite membranes. FTIR spectra corresponding to the white crosses positions located in the PCA images of the composite membranes: c) solution impregnated (C-IMP) and d) solution mixed (C-MEZC). The concentration of PK50IM80 increases in the color order: blue < green < red.

diffraction peak was observed that would indicate the presence of crystalline PK50IM80 suggesting that it is present in its amorphous form.

Fig. 6 shows optical and FTIR images from the surface of the composite membranes (C-IMP and C-MEZC). For C-IMP, one can see that P50IM80 polymer was distributed homogeneously on the membrane surface (green zones). A few blue zones were observed, which corresponded to low concentration areas of PK50IM80. For C-MEZC, a higher number of more agglomerated blue pixels indicated that PK50IM80 was not as well homogeneously dispersed at the surface of the membrane as compared to C-IMP. This result suggested that the solution impregnation method promotes a more homogeneous distribution of PK50IM80 on the surface of the composite membranes. On the other hand, the mixing method apparently promoted deeper intercalation and possible entanglement of PK50IM80 along the thickness of the cellulose membrane.

Fig. 7a–b shows 2D chemical images obtained by principal component analysis (PCA). The surface of the composite membranes prepared by solution impregnation (C-IMP) exhibited a more homogeneous distribution of PK50IM80 as compared to the composite membranes prepared by solution mixing (C-MEZC). The green and red colors corresponded to regions with high concentration of PK50IM80 whereas the blue color corresponds to regions with lower amounts of PK50IM80.

Fig. 8 shows scanning electron micrographs obtained from the surface of MFC (C-1) and the composite membranes (C-IMP and C-MEZC). From Fig. 8a and b, it is possible to observe that the respective surfaces of C-1 and C-IMP were constituted mainly of a highly dense network of fibres. This was also suggested by AFM images (Figs. S7 and S8). A few pores could be observed as indicated by the white arrows (Fig. 8a–c). Fig. 8c shows that the surface of C-MEZC composite membranes was mainly constituted of a highly dense fibres network with a more porous structure in some areas. In Fig. 8b the width of CNFs is indicated. This range started from ~7 nm and finishes at ~140 nm, which was in good agreement with the estimation obtained by AFM imaging (compare Fig. 2). As a whole, SEM imaging suggested that the presence of PK50IM80 did not affect the surface morphology of MFC fibres, which was also suggested by AFM imaging (compare Figs. S7 and S8). This agreed with the fact that a low weight fraction of PK50IM80 was introduced into the composite membranes (3.8 ± 0.01% and 1.7 ± 0.01% for C-IMP and C-MEZC, respectively). The surface composition of MFC membranes as well as C-IMP and C-MEZC composite membranes was identified by EDX. The results are reported in Table S4 and indicate the presence of nitrogen for both C-IMP and C-MEZC. This was related to the presence of PK50IM80, which was successfully deposited at the surface and intercalated within MFC fibres.

Thermograms of MFC membranes (C-1) and composite membranes (C-IMP and C-MEZC) are shown in Fig. S9 and corresponding DTG curves in Fig. S9b. C-1, C-IMP and C-MEZC exhibited three thermal degradation stages. The first thermal stage corresponded to a weight loss of ~5% starting at about 50 °C and finishing at ~200 °C. This was mainly associated with the loss of moisture from the membranes. A second thermal event was identified with an onset at a temperature of 200–230 °C, with its maximum of the DTG curve at about 330 °C, corresponding to the main weight loss as reported in Table S5. This weight

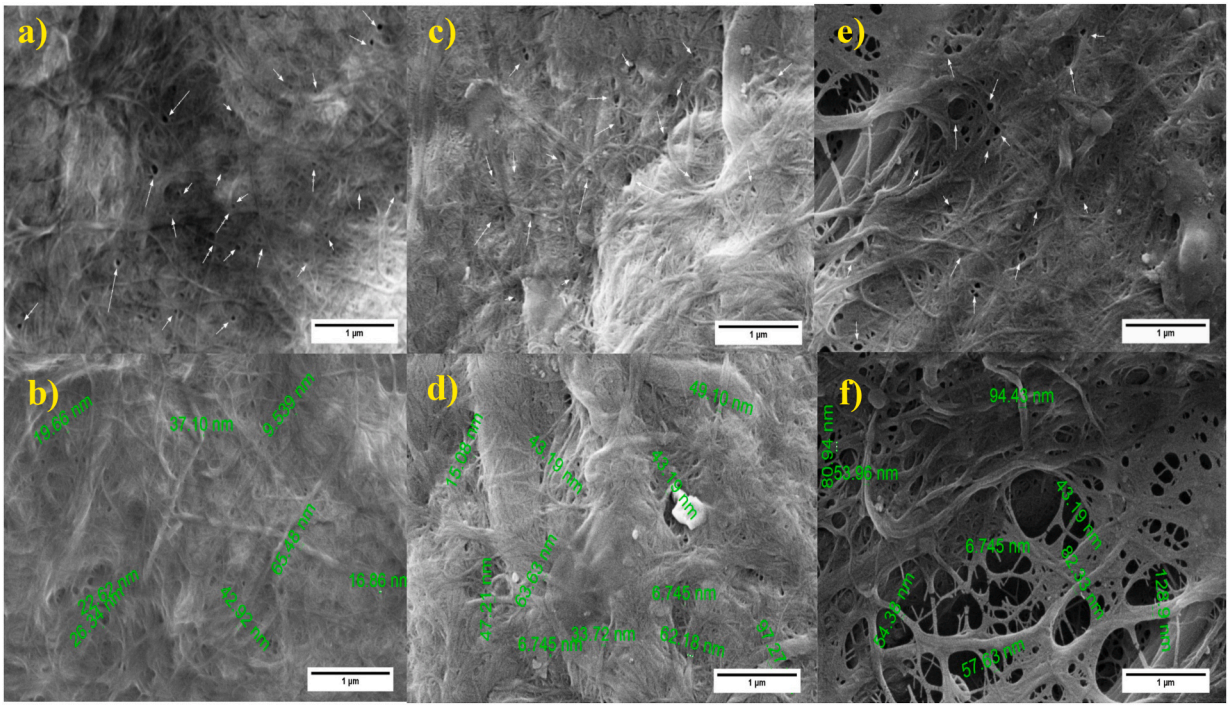

Fig. 8. Scanning electron microscopy (SEM) images obtained from the surface of (a-b) microfibrillated cellulose membrane (C-1), composite membranes prepared by (c-d) solution impregnation (C-IMP) and (e-f) solution mixing (C-MEZC). The small white arrows (a, c and e) indicate the presence of pores at the membrane surface. Scale bars correspond to 1 µm. Dimensions indicated in b) correspond to the width of cellulose nanofibers whereas in d) and f) they correspond to the width of cellulose nanofibers covered by the chemically modified polyketone matrix.

Table 2
Storage modulus and glass transition temperature (T_g) obtained from dynamic mechanical analysis for microfibrillated cellulose membranes (C-1) and as composite membranes prepared by solution impregnation (C-IMP) and solution mixing (C-MEZC).

Material	Storage modulus (GPa) at 25 °C	T_g (°C)
C-1	5.4	–
C-IMP	6.7	50
C-MEZC	4.6	60

loss corresponded to the thermal degradation of cellulose and PK50IM80. Finally, a third thermal stage was found to occur over a temperature range between 350 and 600 °C. No thermal event was observed above 600 °C.

Dynamic mechanical analysis (DMA) was utilized to study the thermomechanical properties of MFC membranes (C-1) and composite membranes (C-IMP and C-MEZC). Figs. S10a and S10b show the storage modulus (E') and the ratio of the dissipated to the stored energy (tanδ), respectively, as a function of temperature. For all membranes, the trend of the storage modulus as a function of temperature was similar. For example, the glassy region as indicated by a drop of the storage modulus was observed in the temperature range of 0–50 °C. A contribution to this loss at 50 °C may be stemming from the presence of moisture, which evaporated from samples. After this, it was observed that the storage modulus decreases both in the glassy region as well as in the rubbery state. At all temperatures (0–200 °C), the storage modulus was significantly higher for C-IMP than for C1, followed by C-MEZC (Table 2, at 25 °C). Interestingly, a plateau was observed for C-IMP and C-1 from ~50 to 100 °C and ~80–140 °C, respectively, where their storage modulus remained almost constant. On the other hand, for C-MEZC, the storage modulus steadily decreased upon increasing temperature. At 200 °C, the storage modulus of C-IMP remained higher than for C-1 and C-MEZC. The higher storage modulus values of C-IMP as compared to C-1 and C-MEZC may have arisen from several reasons. First of all, PK50IM80 was

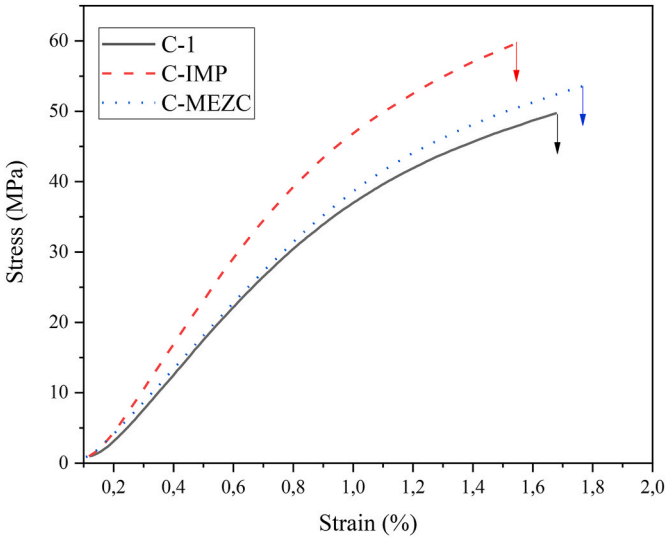

Fig. 9. Representative stress-strain curves of microfibrillated cellulose membrane (C-1, black full line) and composite membranes prepared by solution impregnation (C-IMP, red dashed line) and solution mixing (C-MEZC, blue dotted line).

found to be more homogeneously distributed on the surface of C-IMP membranes compared to C-MEZC. Another explanation must be related to the composite preparation method, for which it is believed that the solution impregnation method preserves the hydrogen bonding of the MFC fibre network, whereas during the solution mixing method the presence of PK50IM80 throughout the MFC fibre network hindered the hydrogen bonding between MFC fibres, resulting in lowered the storage modulus of C-MEZC compared to C-IMP.

The tanδ values of MFC membranes (C-1) and composite membranes

Table 3
Tensile mechanical properties and specific surface area values for MFC (C-1) and composite membranes prepared by impregnation (C-IMP) and mixing (C-MEZC) methods.

Material	Young's modulus (GPa)	Stress at failure (MPa)	Strain at failure (%)	Work of fracture (MJ m^{-3})	Tensile index (Nm g^{-1})	Specific surface area (m^2 g^{-1})
C-1	4.5 ± 0.5	49.7 ± 2.2	1.7 ± 0.3	0.5 ± 0.1	63.6 ± 1.3	1.13
C-IMP	5.9 ± 0.3	60.1 ± 4.6	1.5 ± 0.2	0.5 ± 0.2	51.9 ± 2.2	1.24
C-MEZC	4.4 ± 0.2	54.9 ± 2.7	1.8 ± 0.3	0.6 ± 0.1	57.6 ± 2.2	1.20

(C-IMP and C-MEZC) as a function of temperature are reported in Fig. S10b. One can see that combining PK50IM80 with MFC fibres decreased tanδ values, particularly for C-MEZC compared to C-IMP. This suggests that C-IMP membranes possessed better ability to dissipate energy than C-MEZC membranes.

Fig. 9 shows stress-strain curves for MFC membranes (C-1) and composite membranes (C-IMP and C-MEZC). The detailed mechanical properties are reported in Table 3. One can see that the Young's modulus of C-IMP is significantly higher than for C-1 and C-MEZC, which was in good agreement with storage modulus data obtained by DMA. Also, C-IMP and C-MEZC possessed significantly higher stress at failure (without significant difference between them) compared to C-1. Strain at failure as well as work of fracture did not significantly change upon addition of PK50IM80 to MFC fibres. Values of work of fracture have been related to a layer-to-layer delamination deformation mechanism of a form of layered composites [49]. In the present study, this mechanism was also present as shown by SEM images, where delamination between the layers constituting MFC membranes (C-1) and composite membranes (C-IMP and C-MEZC) occurred (Fig. S11). The presence of PK50IM80 did not seem to either prevent nor favour their deformation mechanism by delamination as suggested by strain at failure and work of fracture data showing no significant difference between C-1, C-IMP and C-MEZC.

The significantly higher Young's modulus of C-IMP compared to C-1 and C-MEZC may be governed by how well the fibre/fibre hydrogen bonding interactions between the MFC fibres constituting the network can be preserved during the manufacturing process and, as a result, may maintain the stress transfer ability of the MFC network present in the composite material. In a previous work, MFC/polylactic acid (PLA) laminated composites were fabricated and their stress transfer efficiency was found to be dominated by the MFC network rather than at the interface between PLA and the surface of the MFC network as quantified by Raman spectroscopy [28]. The presence of PK50IM80 located mainly at the surface of C-IMP, as suggested by FTIR 2D imaging, might have played a role in the consolidation of the network structure where MFC fibres located at the surface bound together during fabrication. Similar behaviour has previously been observed for BC/PLA laminated composites [32]. The significantly lower Young's modulus of C-MEZC compared to C-IMP may be due to disruption of the strong attractive hydrogen bonding that normally form within the MFC fibre network due to the presence of PK50IM80 throughout the bulk membrane structure. This has been suggested to occur for BC/PVA nanocomposites [25]. Instead, C-IMP seems to behave like a laminated composite system, which contributes to significantly increase Young's modulus while maintaining tensile strength [28,33]. Tensile index values of C-1, C-IMP and C-MEZC are reported in Table 3, which is a way to normalize tensile strength values with respect to grammage. C-1 possessed significantly higher tensile index than C-IMP and C-MEZC. This is mainly because C-1 possessed significantly lower grammage than C-IMP and C-MEZC as reported in Table S1. The higher grammage values of C-IMP and C-MEZC did originate from the incorporation of PK50IM80 within their network structure.

Table 3 reports specific surface area values determined by iGC for MFC membranes (C-1) and composite membranes (C-IMP and C-MEZC). These values, although quite low, were not found to be significantly affected by the presence of PK50IM80, confirming the hypothesis of maintained pore structure.

Fig. 10 shows streaming zeta-potential (ζ) data obtained for MFC membranes (C-1) and composite membranes (C-IMP and C-MEZC) as a function of pH. For C-1, the trend was similar to data reported before for a range of cellulose membranes, including phosphorylated cellulose nanofibre (CNF) membranes [50], bacterial cellulose (BC) as well as TEMPO-oxidized CNF membranes [22]. The zeta potential value of C-1 was positive (~5 mV) at pH ~2, and decreases upon pH increase,

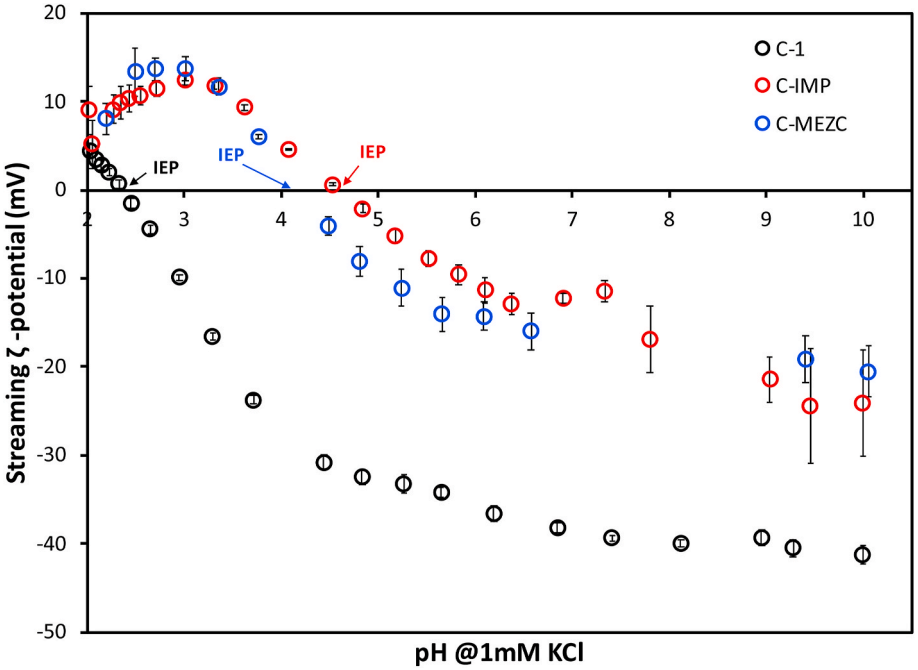

Fig. 10. Zeta-potential (ζ) as a function of pH as measured by streaming potential measurements for MFC (C-1) and composite (C-IMP and C-MEZC) membranes.

reaching the isoelectric point (IEP) at pH ~2.4. This lowered zeta potential value was due to the gradual deprotonation of acidic moieties present at the surface of MFC fibres [22]. At pH > 2.4 the zeta potential values became more negative, reaching a plateau value of ~ −40 mV at pH ~7.5. This magnitude of the zeta potential plateau was higher than reported in previous works with plateau values of ~ −26 mV for TEMPO oxidized-CNF [22] and ~−20 mV reached for BC [22], which were also reached at a pH ~7.5.

For C-IMP and C-MEZC, the trend differed from C-1. When pH was increased from 2 to 3, zeta potential values increased from ~5 up to 15 mV. In a previous work, it has been reported that imidazole groups grafted onto pendant groups of PK50 exhibited positive surface charge (cationic behaviour) under acidic conditions [37]. The magnitude of the positive surface charge was found to increase upon increasing the pH from ~3 to 7 [37]. At pH > 3, the zeta potential values started decreasing due to the gradual deprotonation of acidic moieties that belong to MFC fibres. The IEP was reached at pH ~4.5 and 4.2 for C-IMP and C-MEZC, respectively. Thus, the presence of PK50IM80 significantly shifted the IEP from ~2.4 (for C-1) up to 4.5 (for C-IMP) due to the presence of imidazole groups acting as weak acids. These groups induced a charge compensation effect to the MFC fibres. Isoelectric points close to 4.5 have been reported for polymeric membranes based on polyamide [51], polyacrylonitrile [52] or polyamidoamine [53], similarly to our C-IMP composite membrane.

At pH > IEP, the zeta potential values of C-IMP and C-MEZC became negative, reaching minimum values of ~ −24.1 ± 6 mV and ~−20.5 ± 2.9 mV at pH 10, respectively. These plateau values were close to values reported before for TEMPO-CNF membranes [22]. This decrease of zeta potential values was due to the gradual deprotonation of moieties that belong to MFC fibres but also to the deprotonation of cationic to neutral moieties of imidazole groups in the PK50IM80 upon increasing pH [54]. These plateau values of −24 mV and −21 mV were lower than for C-1, which further revealed that a charge compensation effect occurred affecting the electrical surface charges of MFC fibres due to the presence of imidazole groups that reduce the magnitude of the lower negative electrical surface charge at the composite membranes' surface.

4. Conclusions

In this work, microfibrillated cellulose (MFC)/imidazole-modified polyketone (PK50IM80) composite membranes were prepared and characterized. MFC was produced by high-pressure homogenization and used to prepare MFC membranes (C-1) by vacuum filtration and hot pressing. PK50 was chemically modified by Paal-Knorr reaction leading to the introduction of imidazole functional groups within the molecular structure of PK. The resulting modified PK was referred to as PK50IM80. MFC/PK50IM80 composite membranes were fabricated by two methods: solution impregnation and solution mixing. The resulting composite membranes were named C-IMP and C-MEZC, respectively. The surfaces of C-IMP and C-MEZC were imaged by FTIR microscopy. The results suggested that a more homogeneous distribution of PK50IM80 at the surface of MFC was obtained using solution impregnation method. The successful deposition of PK50IM80 was further confirmed by identifying (EDX) and quantifying (XPS) the nitrogen atoms present at the surface of the composite membranes. Their thermal properties were also investigated by TGA and DMA. TGA suggested that MFC and composite membranes possessed similar thermal stability. The mechanical properties of MFC and composite membranes were determined by dynamical mechanical analysis and tensile tests. Both techniques revealed that C-IMP possessed significantly higher stiffness than C-1 and C-MEZC. Tensile testing demonstrated that C-IMP had significantly higher tensile strength compared to C-1 whereas strain at failure as well as work of fracture were similar for all materials. Also, C-1 was found to possess a significantly higher tensile index value compared to C-IMP and C-MEZC. The deposition of PK50IM80 onto MFC was not found to significantly affect specific surface area. The amplitude of the electrical surface charges of MFC and C-IMP and C-MEZC membranes were quantified by streaming zeta-potential as a function of pH. Composite membranes were found to possess an isoelectric point (IEP) at pH ~4.5, close to IEP values reported before for polyamide, polyacrylonitrile or polyamidoamine composite membranes. MFC membranes were found to possess an IEP at pH ~2.4. Also, at pH > IEP, composite membranes were found to possess lower negative surface charges (down to ~ −22 mV) than MFC membranes (down to ~ −41 mV). We showed that by combining MFC with controlled amounts of PK50IM80, it was possible to tune the mechanical properties, control the magnitude of the negative electrical surface charges of the resulting composite membranes as well as shifting their isoelectric point from 2.4 to 4.5. Our approach paves a new way to adjust the surface properties of MFC-based membranes. These could be used as filtration membrane for the selective removal of a wide range of chemical species from water including metallic cations.

Data availability

The raw/processed data required to reproduce these findings cannot be shared at this time due to technical or time limitations.

Declaration of competing interest

The authors declare that they have no known competing financial interests or personal relationships that could have influenced the work reported in this paper.

CRediT authorship contribution statement

Pablo Gonzalez Cortes: Investigation, Funding acquisition, Writing - original draft. **Rodrigo Araya-Hermosilla:** Conceptualization, Investigation, Supervision, Writing - original draft, Writing - review & editing. **Esteban Araya-Hermosilla:** Investigation. **Daniela Acuña:** Investigation. **Andreas Mautner:** Investigation, Writing - review & editing. **Leonardo Caballero:** Investigation. **Francisco Melo:** Resources, Writing - review & editing. **Ignacio Moreno Villoslada:** Resources. **Francesco Picchioni:** Resources. **Aldo Rolleri:** Investigation, Resources. **Franck Quero:** Conceptualization, Resources, Funding acquisition, Supervision, Writing - original draft, Writing - review & editing.

Acknowledgements

The authors are grateful to the support of the Programa Formación de Capital Humano Avanzado, Conicyt, Becas Chile; Grant N° 21170475. The authors are also thankful to Carla Herrera Cantera, Research Assistant of the Programa Institucional de Fomento a la Investigacion, Desarrollo e Innovacion (PIDI), Universidad Tecnológica Metropolitana, San Joaquin, Santiago, Chile. Thanks to FONDEQUIP Grants N° EQM130149, EQM150019, EQM150101 and EQM190177. Acknowledgments are also extended to the "Nuclei for Smart Soft Mechanical Metamaterials" grant funded by the Millennium Science Initiative of the Ministry of Economy, Development and Tourism. F. M. acknowledges Dicyt-Usach through project No 041831MH-Postdoc. Thank you to Dr. Nathan Kirchhofer (Asylum Research – an Oxford Instruments Company, Santa Barbara, CA) for his assistance in acquiring AFM images of the surface of MFC and composite membranes. Jorge Luengo (CMPC, Nacimiento, Chile) is acknowledged for supplying the commercial bleached eucalyptus cellulose pulp.

Appendix A. Supplementary data

Supplementary data to this article can be found online at https://doi.org/10.1016/j.polymertesting.2020.106710.

References

[1] S.J. Eichhorn, S.S. Rahatekar, S. Vignolini, A.H. Windle, New horizons for cellulose nanotechnology, Philos. Trans. R. Soc. A Math. Phys. Eng. Sci. 376 (2018), 20170200, https://doi.org/10.1098/rsta.2017.0200.

[2] L.A. Berglund, T. Peijs, Cellulose biocomposites—from bulk moldings to nanostructured systems, MRS Bull. 35 (2010) 201–207, https://doi.org/10.1557/mrs2010.652.

[3] D. Klemm, B. Heublein, H.-P. Fink, A. Bohn, Cellulose: fascinating biopolymer and sustainable raw material, Angew. Chem. Int. Ed. 44 (2005) 3358–3393, https://doi.org/10.1002/anie.200460587.

[4] A.F. Turbak, F.W. Snyder, K.R. Sandberg, Microfibrillated cellulose, a new cellulose product: properties, uses, and commercial potential, in: J. Appl. Polym. Sci.: Appl. Polym. Symp, 1983. United States, https://www.osti.gov/servlets/purl/5062478.

[5] S.H. Osong, S. Norgren, P. Engstrand, Processing of wood-based microfibrillated cellulose and nanofibrillated cellulose, and applications relating to papermaking: a review, Cellulose 23 (2016) 93–123, https://doi.org/10.1007/s10570-015-0798-5.

[6] F.W. Herrick, R.L. Casebier, J.K. Hamilton, K.R. Sandberg, Microfibrillated cellulose: morphology and accessibility, in: J. Appl. Polym. Sci.: Appl. Polym. Symp, 1983. United States, https://www.osti.gov/servlets/purl/5039044.

[7] P.A. Larsson, A. V Riazanova, G. Cinar Ciftci, R. Rojas, H.H. Øvrebø, L. Wågberg, L. A. Berglund, Towards optimised size distribution in commercial microfibrillated cellulose: a fractionation approach, Cellulose 26 (2019) 1565–1575, https://doi.org/10.1007/s10570-018-2214-4.

[8] W.J. Fischer, M. Mayr, S. Spirk, D. Reishofer, L.A. Jagiello, R. Schmiedt, J. Colson, A. Zankel, W. Bauer, Pulp fines-characterization, sheet formation, and comparison to microfibrillated cellulose, Polymers 9 (2017) 366, https://doi.org/10.3390/polym9080366.

[9] H. Jin, Y. Nishiyama, M. Wada, S. Kuga, Nanofibrillar cellulose aerogels, Colloids Surf A Physicochem. Eng. Asp. 240 (2004) 63–67, https://doi.org/10.1016/j.colsurfa.2004.03.007.

[10] K.J. De France, T. Hoare, E.D. Cranston, Review of hydrogels and aerogels containing nanocellulose, Chem. Mater. 29 (2017) 4609–4631, https://doi.org/10.1021/acs.chemmater.7b00531.

[11] J. Yao, S. Chen, Y. Chen, B. Wang, Q. Pei, H. Wang, Macrofibers with high mechanical performance based on aligned bacterial cellulose nanofibers, ACS Appl. Mater. Interfaces 9 (2017) 20330–20339, https://doi.org/10.1021/acsami.6b14650.

[12] S.J. Eichhorn, A. Dufresne, M. Aranguren, N.E. Marcovich, J.R. Capadona, S. J. Rowan, C. Weder, W. Thielemans, M. Roman, S. Renneckar, W. Gindl, S. Veigel, J. Keckes, H. Yano, K. Abe, M. Nogi, A.N. Nakagaito, A. Mangalam, J. Simonsen, A. S. Benight, A. Bismarck, L.A. Berglund, T. Peijs, Review: current international research into cellulose nanofibres and nanocomposites, J. Mater. Sci. 45 (2010) 1–33, https://doi.org/10.1007/s10853-009-3874-0.

[13] A. Mautner, Nanocellulose water treatment membranes and filters: a review, Polym. Int. (2020), https://doi.org/10.1002/pi.5993.

[14] I. González, M. Alcalà, G. Chinga-Carrasco, F. Vilaseca, S. Boufi, P. Mutjé, From paper to nanopaper: evolution of mechanical and physical properties, Cellulose 21 (2014) 2599–2609, https://doi.org/10.1007/s10570-014-0341-0.

[15] A.N. Nakagaito, H. Yano, The effect of fiber content on the mechanical and thermal expansion properties of biocomposites based on microfibrillated cellulose, Cellulose 15 (2008) 555–559, https://doi.org/10.1007/s10570-008-9212-x.

[16] H. Fukuzumi, T. Saito, T. Iwata, Y. Kumamoto, A. Isogai, Transparent and high gas barrier films of cellulose nanofibers prepared by TEMPO-mediated oxidation, Biomacromolecules 10 (2009) 162–165, https://doi.org/10.1021/bm801065u.

[17] S.S. Nair, J.Y. Zhu, Y. Deng, A.J. Ragauskas, High performance green barriers based on nanocellulose, Sustain. Chem. Process. 2 (2014) 23, https://doi.org/10.1186/s40508-014-0023-0.

[18] A. Mautner, K.-Y. Lee, T. Tammelin, A.P. Mathew, A.J. Nedoma, K. Li, A. Bismarck, Cellulose nanopapers as tight aqueous ultra-filtration membranes, React. Funct. Polym. 86 (2015) 209–214, https://doi.org/10.1016/j.reactfunctpolym.2014.09.014.

[19] A.W. Carpenter, C.-F. de Lannoy, M.R. Wiesner, Cellulose nanomaterials in water treatment technologies, Environ. Sci. Technol. 49 (2015) 5277–5287, https://doi.org/10.1021/es506351r.

[20] H. Voisin, L. Bergström, P. Liu, P.A. Mathew, Nanocellulose-based materials for water purification, Nanomaterials 7 (2017) 57, https://doi.org/10.3390/nano7030057.

[21] A. Mautner, T. Kobkeatthawin, F. Mayer, C. Plessl, S. Gorgieva, V. Kokol, A. Bismarck, Rapid water softening with TEMPO-oxidized/phosphorylated nanopapers, Nanomaterials 9 (2019) 136, https://doi.org/10.3390/nano9020136.

[22] A. Mautner, M. Hakalahti, V. Rissanen, T. Tammelin, Crucial interfacial features of nanocellulose materials, in: Koon-Yang Lee (Ed.), Nanocellulose and Sustainability: Production, Properties, Applications, and Case Studies, CRC Press, Boca Raton, 2018, pp. 85–127.

[23] Y.-L. Ji, B.-X. Gu, Q.-F. An, C.-J. Gao, Recent advances in the fabrication of membranes containing “Ion Pairs” for nanofiltration processes, Polymer 9 (2017) 115, https://doi.org/10.3390/polym9120715.

[24] H. Ma, B.S. Hsiao, B. Chu, in: E. Drioli, L. Giorno (Eds.), Modified Cellulose BT - Encyclopedia of Membranes, Springer Berlin Heidelberg, Berlin, Heidelberg, 2016, pp. 1320–1321, https://doi.org/10.1007/978-3-662-44324-8_390.

[25] S. Gea, E. Bilotti, C.T. Reynolds, N. Soykeabkeaw, T. Peijs, Bacterial cellulose–poly (vinyl alcohol) nanocomposites prepared by an in-situ process, Mater. Lett. 64 (2010) 901–904, https://doi.org/10.1016/j.matlet.2010.01.042.

[26] K. Oksman, Y. Aitomäki, A.P. Mathew, G. Siqueira, Q. Zhou, S. Butylina, S. Tanpichai, X. Zhou, S. Hooshmand, Review of the recent developments in cellulose nanocomposite processing, Compos. Part A Appl. Sci. Manuf. 83 (2016) 2–18, https://doi.org/10.1016/j.compositesa.2015.10.041.

[27] M. Nogi, S. Iwamoto, A.N. Nakagaito, H. Yano, Optically transparent nanofiber paper, Adv. Mater. 21 (2009) 1595–1598, https://doi.org/10.1002/adma.200803174.

[28] S. Tanpichai, W.W. Sampson, S.J. Eichhorn, Stress-transfer in microfibrillated cellulose reinforced poly(lactic acid) composites using Raman spectroscopy, Compos. Part A Appl. Sci. Manuf. 43 (2012) 1145–1152, https://doi.org/10.1016/j.compositesa.2012.02.006.

[29] A. Chakrabarty, Y. Teramoto, Recent advances in nanocellulose composites with polymers: a guide for choosing partners and how to incorporate them, Polymer 10 (2018) 517, https://doi.org/10.3390/polym10050517.

[30] Y. Habibi, A. Dufresne, Highly filled bionanocomposites from functionalized polysaccharide nanocrystals, Biomacromolecules 9 (2008) 1974–1980, https://doi.org/10.1021/bm8001717.

[31] K.-Y. Lee, Y. Aitomäki, L.A. Berglund, K. Oksman, A. Bismarck, On the use of nanocellulose as reinforcement in polymer matrix composites, Compos. Sci. Technol. 105 (2014) 15–27, https://doi.org/10.1016/j.compscitech.2014.08.032.

[32] K.-Y. Lee, J.J. Blaker, A. Bismarck, Surface functionalisation of bacterial cellulose as the route to produce green polylactide nanocomposites with improved properties, Compos. Sci. Technol. 69 (2009) 2724–2733, https://doi.org/10.1016/j.compscitech.2009.08.016.

[33] F. Quero, M. Nogi, H. Yano, K. Abdulsalami, S.M. Holmes, B.H. Sakakini, S. J. Eichhorn, Optimization of the mechanical performance of bacterial cellulose/poly(l-lactic acid) composites, ACS Appl. Mater. Interfaces 2 (2010) 321–330, https://doi.org/10.1021/am900817f.

[34] W. Gindl, J. Keckes, Tensile properties of cellulose acetate butyrate composites reinforced with bacterial cellulose, Compos. Sci. Technol. 64 (2004) 2407–2413, https://doi.org/10.1016/j.compscitech.2004.05.001.

[35] H. Dong, Y.R. Sliozberg, J.F. Snyder, J. Steele, T.L. Chantawansri, J.A. Orlicki, S. D. Walck, R.S. Reiner, A.W. Rudie, Highly transparent and toughened poly(methyl methacrylate) nanocomposite films containing networks of cellulose nanofibrils, ACS Appl. Mater. Interfaces 7 (2015) 25464–25472, https://doi.org/10.1021/acsami.5b08317.

[36] W.P. Mul, H. Dirkzwager, A.A. Broekhuis, H.J. Heeres, A.J. van der Linden, A. Guy Orpen, Highly active, recyclable catalyst for the manufacture of viscous, low molecular weight, CO–ethene–propene-based polyketone, base component for a new class of resins, Inorg. Chim. Acta. 327 (2002) 147–159, https://doi.org/10.1016/S0020-1693(01)00697-1.

[37] E. Araya-Hermosilla, S.L. Orellana, C. Toncelli, F. Picchioni, I. Moreno-Villoslada, Novel polyketones with pendant imidazolium groups as nanodispersants of hydrophobic antibiotics, J. Appl. Polym. Sci. 132 (2015), https://doi.org/10.1002/app.42363.

[38] R. Araya-Hermosilla, G.M.R. Lima, P. Raffa, G. Fortunato, A. Pucci, M.E. Flores, I. Moreno-Villoslada, A.A. Broekhuis, F. Picchioni, Intrinsic self-healing thermoset through covalent and hydrogen bonding interactions, Eur. Polym. J. 81 (2016) 186–197, https://doi.org/10.1016/j.eurpolymj.2016.06.004.

[39] N. Migliore, M.L. Polgar, R. Araya-Hermosilla, F. Picchioni, P. Raffa, A. Pucci, Effect of the polyketone aromatic pendent groups on the electrical conductivity of the derived MWCNTs-based nanocomposites, Polymer 10 (2018) 618, https://doi.org/10.3390/polym10060618.

[40] Y. Zhang, A.A. Broekhuis, M.C.A. Stuart, F. Picchioni, Polymeric amines by chemical modifications of alternating aliphatic polyketones, J. Appl. Polym. Sci. 107 (2008) 262–271, https://doi.org/10.1002/app.27029.

[41] P.A. Figaroa, M. Henk, E. Gert-Jan, P. Francesco, Functional polyketones for the removal of calcium and magnesium from water (part I): synthesis and chemical characterization, Pure Appl. Chem. 89 (2017) 41, https://doi.org/10.1515/pac-2016-1006.

[42] H. Sehaqui, Q. Zhou, O. Ikkala, L.A. Berglund, Strong and tough cellulose nanopaper with high specific surface area and porosity, Biomacromolecules 12 (2011) 3638–3644, https://doi.org/10.1021/bm2008907.

[43] C.C. Sun, Mechanism of moisture induced variations in true density and compaction properties of microcrystalline cellulose, Int. J. Pharm. 346 (2008) 93–101, https://doi.org/10.1016/j.ijpharm.2007.06.017.

[44] I. Siró, D. Plackett, Microfibrillated cellulose and new nanocomposite materials: a review, Cellulose 17 (2010) 459–494, https://doi.org/10.1007/s10570-010-9405-y.

[45] F. Quero, C. Padilla, V. Campos, J. Luengo, L. Caballero, F. Melo, Q. Li, S. J. Eichhorn, J. Enrione, Stress transfer and matrix-cohesive fracture mechanism in microfibrillated cellulose-gelatin nanocomposite films, Carbohydr. Polym. 195 (2018) 89–98, https://doi.org/10.1016/j.carbpol.2018.04.059.

[46] J. Blackwell, Infrared and Raman spectroscopy of cellulose, in: Cellulose Chemistry and Technology, American Chemical Society, 1977, pp. 14–206, https://doi.org/10.1021/bk-1977-0048.ch014.

[47] R. Araya-Hermosilla, A.A. Broekhuis, F. Picchioni, Reversible polymer networks containing covalent and hydrogen bonding interactions, Eur. Polym. J. 50 (2014) 127–134, https://doi.org/10.1016/j.eurpolymj.2013.10.014.

[48] A.D. French, Idealized powder diffraction patterns for cellulose polymorphs, Cellulose 21 (2014) 885–896, https://doi.org/10.1007/s10570-013-0030-4.

[49] F. Quero, S.J. Eichhorn, M. Nogi, H. Yano, K.-Y. Lee, A. Bismarck, Interfaces in cross-linked and grafted bacterial cellulose/poly(lactic acid) resin composites, J. Polym. Environ. 20 (2012) 916–925, https://doi.org/10.1007/s10924-012-0487-5.

[50] A. Mautner, H.A. Maples, T. Kobkeatthawin, V. Kokol, Z. Karim, K. Li, A. Bismarck, Phosphorylated nanocellulose papers for copper adsorption from aqueous

solutions, Int. J. Environ. Sci. Technol. 13 (2016) 1861–1872, https://doi.org/10.1007/s13762-016-1026-z.
[51] H. Zhang, J. Luo, S. Li, Y. Wei, Y. Wan, Biocatalytic membrane based on polydopamine coating: a platform for studying immobilization mechanisms, Langmuir 34 (2018) 2585–2594, https://doi.org/10.1021/acs.langmuir.7b02860.
[52] W.Y. Siew, L.K. Zedda, S. Velizarov, Nanofiltration of simulated acid mine drainage: effect of pH and Membrane Charge, Appl. Sci. 10 (2020), https://doi.org/10.3390/app10010400.
[53] X. Bao, Q. Wu, W. Shi, W. Wang, H. Yu, Z. Zhu, X. Zhang, Z. Zhang, R. Zhang, F. Cui, Polyamidoamine dendrimer grafted forward osmosis membrane with superior ammonia selectivity and robust antifouling capacity for domestic wastewater concentration, Water Res. 153 (2019) 1–10, https://doi.org/10.1016/j.watres.2018.12.067.
[54] A.C.M. Paiva, L. Juliano, P. Boschcov, Ionization of methyl derivatives of imidazole, histidine, thyreotropin releasing factor, and related compounds, J. Am. Chem. Soc. 98 (1976) 7645–7648, https://doi.org/10.1021/ja00440a033.